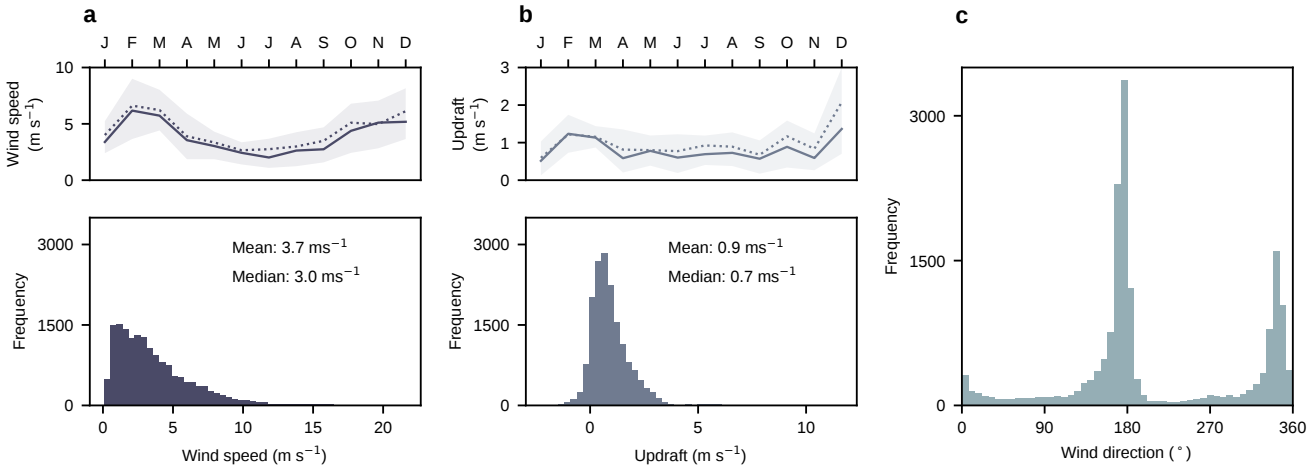

Figure S1. Wind conditions during cloud sampling at Zeppelin Observatory. a–b show monthly averages (upper panels) and histograms (lower panels) of horizontal wind speed and updraft, respectively. For the upper panels in **a–b**, full and dotted lines show median and mean values, respectively, and shaded areas indicate the 25^{th} to 75^{th} percentile ranges. **c** shows a histogram of the wind direction. In all panels, data are only from cloud sampling periods.

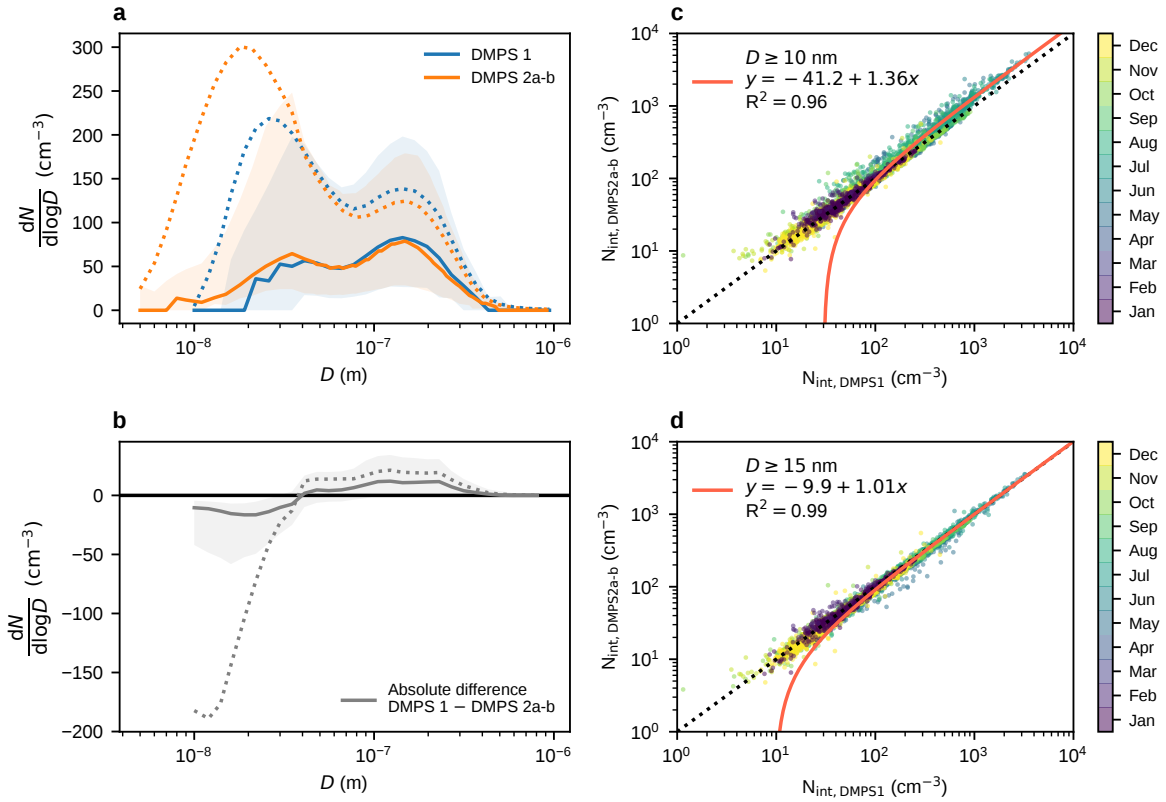

Figure S2. Comparison of particle number size distributions from DMPS 1 and DMPS 2a–b during non-cloud periods. a Particle number size distributions measured with DMPS 1 (blue) and DMPS 2a–b (orange) when measuring on the same inlet. **b** Absolute difference between hourly average particle number size distributions (DMPS 1 minus DMPS 2a–b). For panels **a–b**, full and dotted lines show median and mean values, respectively, and shaded areas indicate the 25^{th} to 75^{th} percentile ranges. Panels **c–d** show scatter plots of hourly average integrated particle number concentrations (integrated above 10 nm and 15 nm particle diameter, respectively) from the DMPS systems, colour coded by month of the year. Red lines show orthogonal distance linear regressions, and black dashed lines indicate the 1:1 relation.

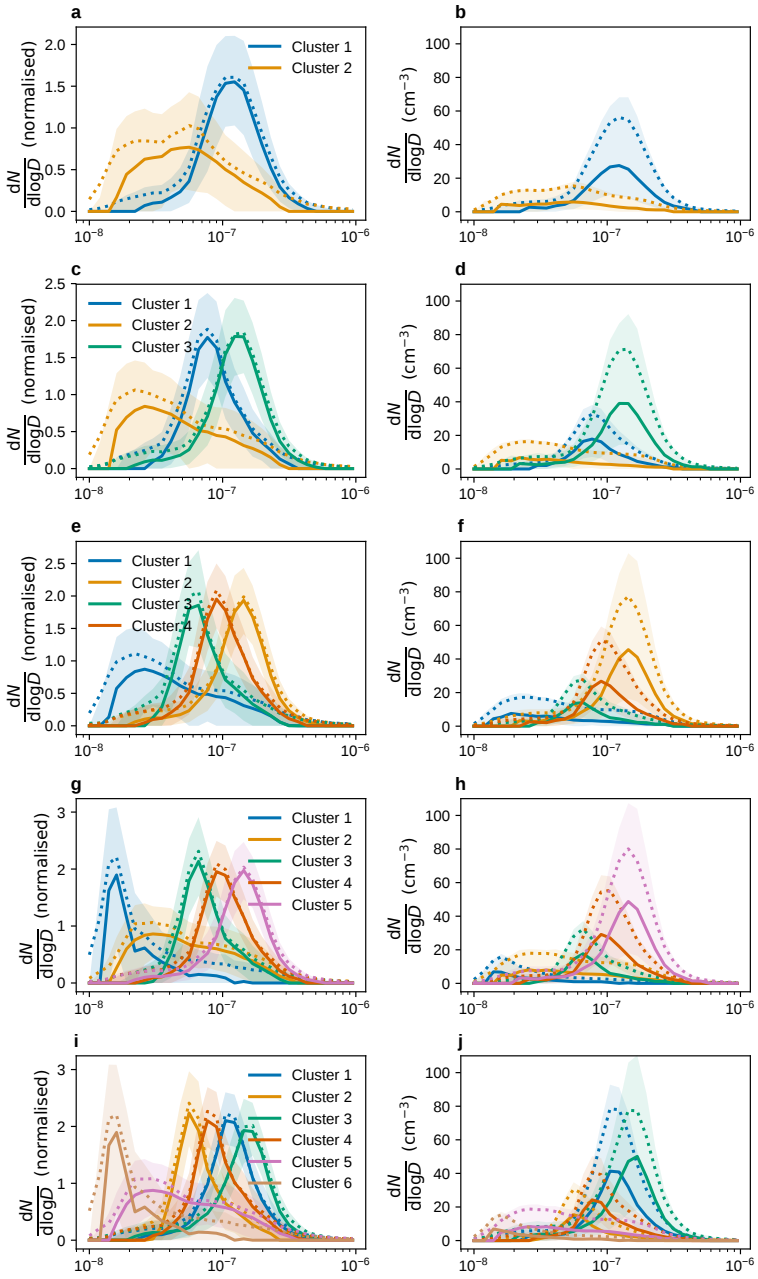

Figure S3. Comparison of different numbers of clusters in k-means. Normalised (left) and non-normalised (right) cloud residual number size distributions resulting from k-means clustering using **a–b** 2 clusters, **c–d** 3 clusters, **e–f** 4 clusters, **g–h** 5 clusters, **i–j** 6 clusters. Solid and dotted lines show median and mean values, respectively, and shaded areas indicate the 25^{th} to 75^{th} percentile ranges.

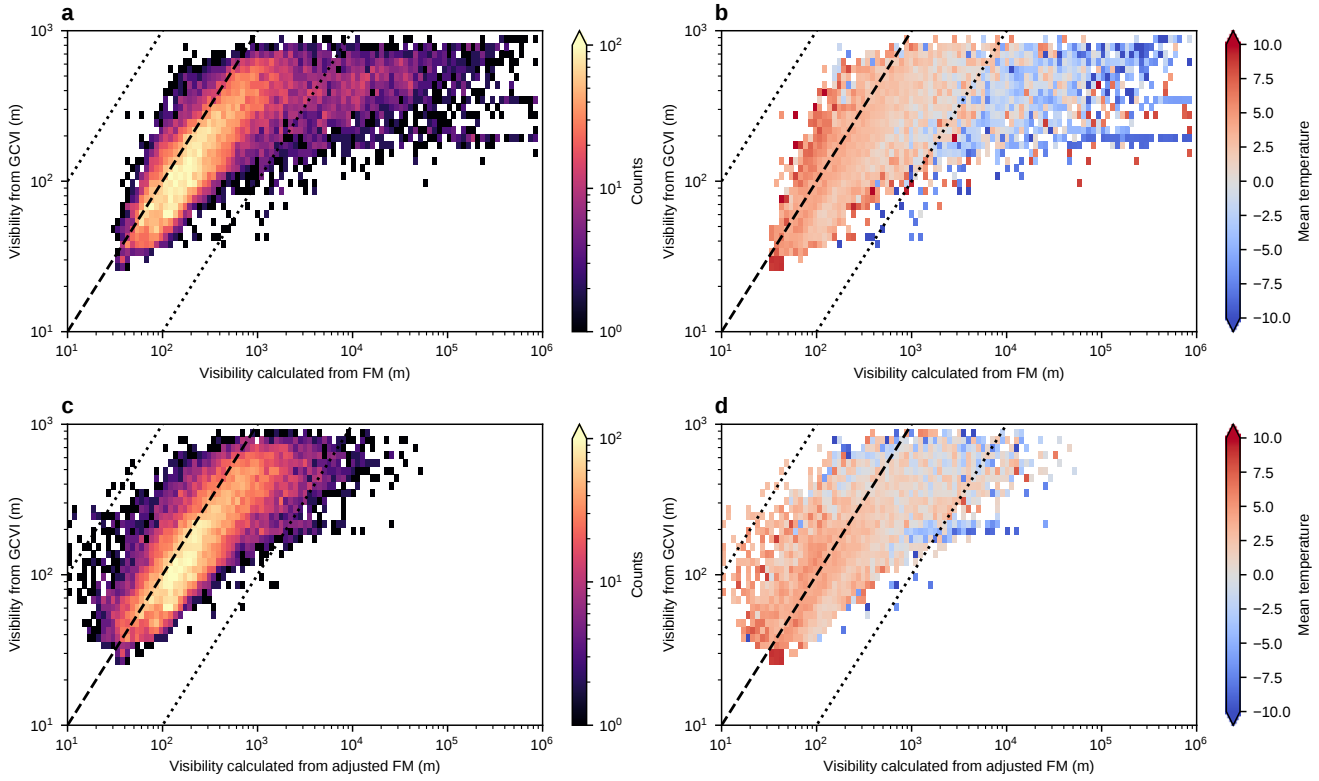

Figure S4. Comparison of measured and calculated visibility. a 2D histogram of visibility as measured by the GCVI visibility sensor (y-axis) versus visibility calculated from the cloud particle size distributions measured by the FM-120 fog monitor (x-axis). **b** Same as a, but colourcoded by temperature instead of data point density. Panels **c** and **d** are the same as a and b, respectively, but the fog monitor concentrations were scaled up to meed cloud residual concentrations (i.e. they were only changed in cases where the cloud residual concentrations exceeded cloud particle concentrations) before the visibility was calculated. Visibility was calculated assuming spherical particles, a refractive index of 1.33, and a wavelength of 880 nm of the visibility sensor.

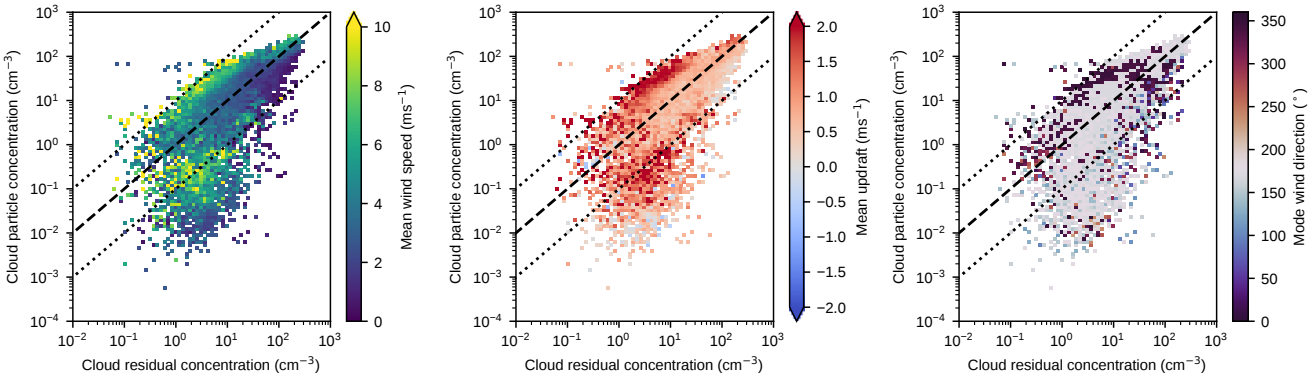

Figure S5. Heatmaps of wind parameters for different cloud residual and cloud particle concentrations. The figure shows heatmaps where cloud residual and cloud particle number concentrations have been cross tabulated with **a** wind speed **b** updraft and **c** wind direction (rounded to the nearest 10 degrees). Note that the pixels do not contain the same number of data points, please refer to Figure 2b in the main manuscript for the corresponding density plot.

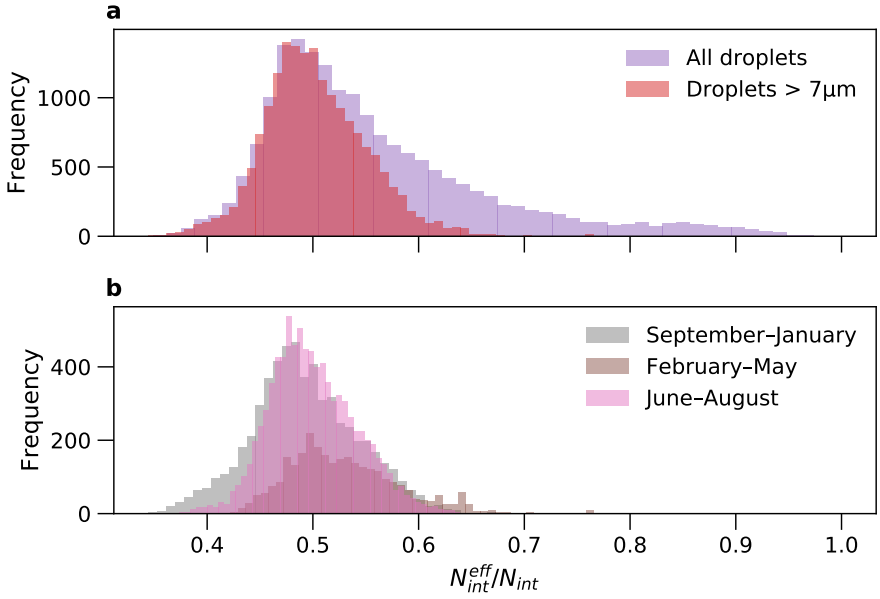

Figure S6. Ratio of ambient cloud particle number concentrations with and without taking the GCVI sampling efficiency into account. Histogram of fog monitor total integrated cloud particle number concentration after correcting for the GCVI transmission efficiency (Shingler et al., 2020) ($N_{\mathrm{int}}^{\mathrm{eff}}$) divided by the total integrated cloud particle number concentration without correction (N_{int}). **a** shows the ratio for the whole cloud particle size range (purple) and when integrating the cloud particle distribution above the GCVI size cut-off (red). **b** shows the red histogram from panel **a** divided into seasons. Assuming there is no correlation between cloud residual size and cloud particle size (and disregarding the sampling efficiency of the FM-120 fog monitor), this ratio can be used to estimate how many of the total number of cloud residuals were actually sampled by the GCVI inlet.

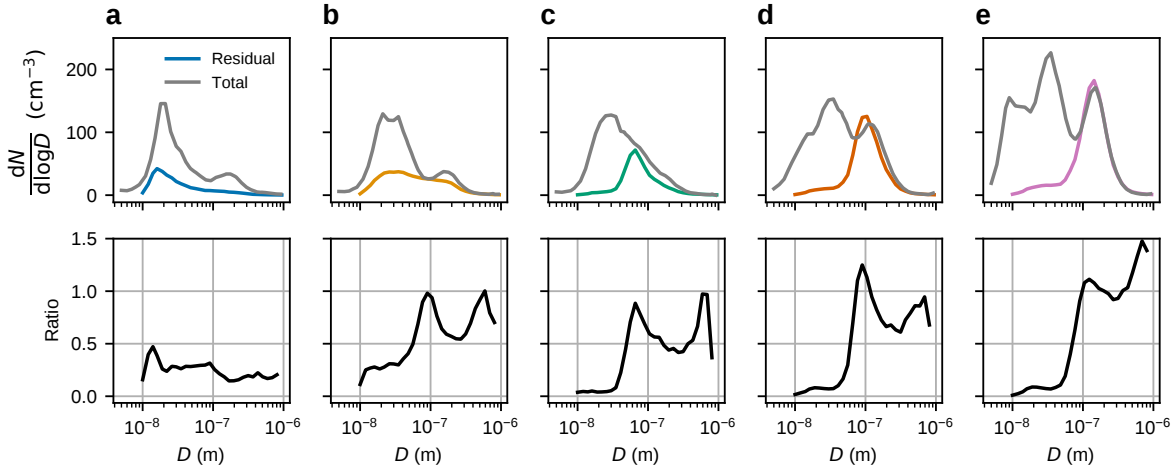

Figure S7. Size distributions and activation ratios for the clusters from Figure 8 in the main manuscript. The top row shows mean cloud residual size distributions (in colour) and the corresponding total particle size distribution (grey). The bottom row shows the corresponding activation ratios. Columns **a–e** show Clusters 1–5, respectively.

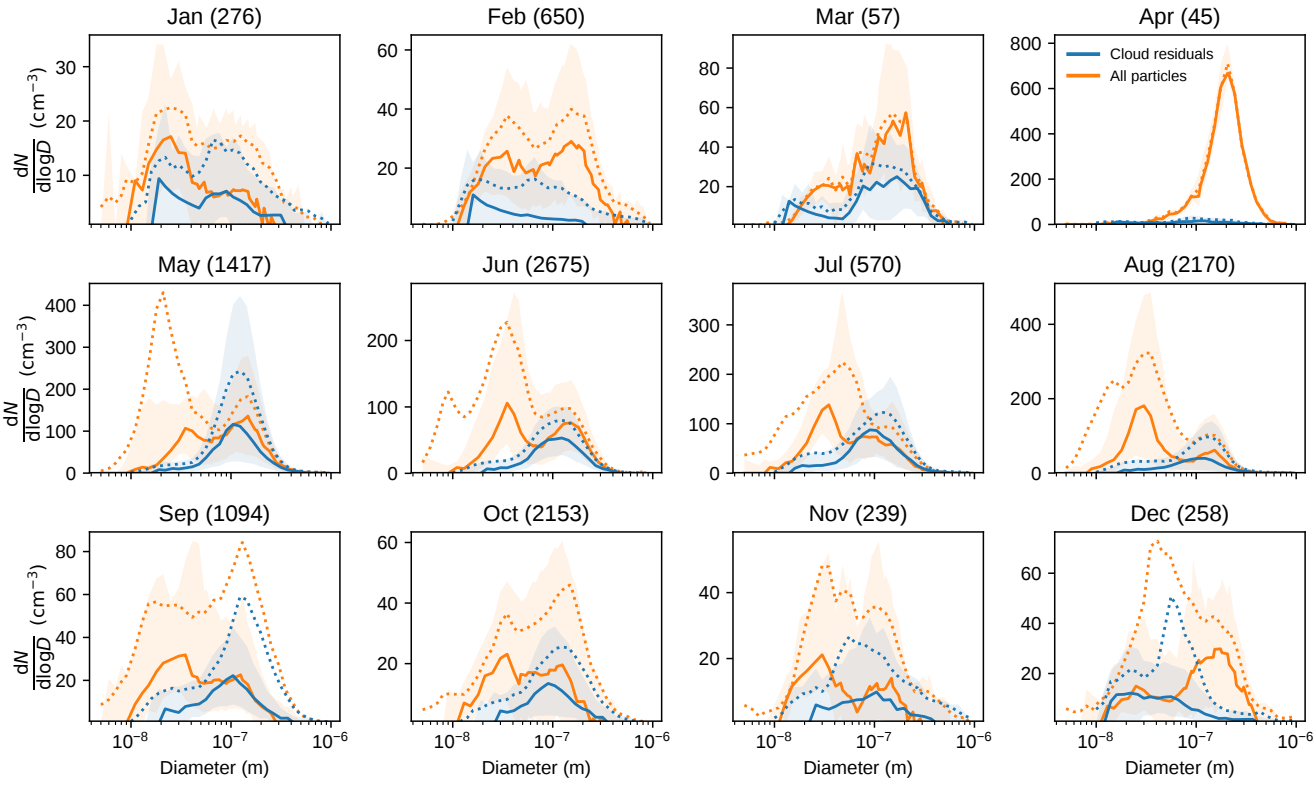

Figure S8. Monthly average particle number size distributions. Concurrent cloud residual (blue) and total particle (orange) particle number size distributions per month. Solid and dotted lines show median and mean values, respectively, and shaded areas indicate the 25$^{\text{th}}$ to 75$^{\text{th}}$ percentile ranges. The numbers in parentheses in the panel headings indicate the number of data points we have per month.

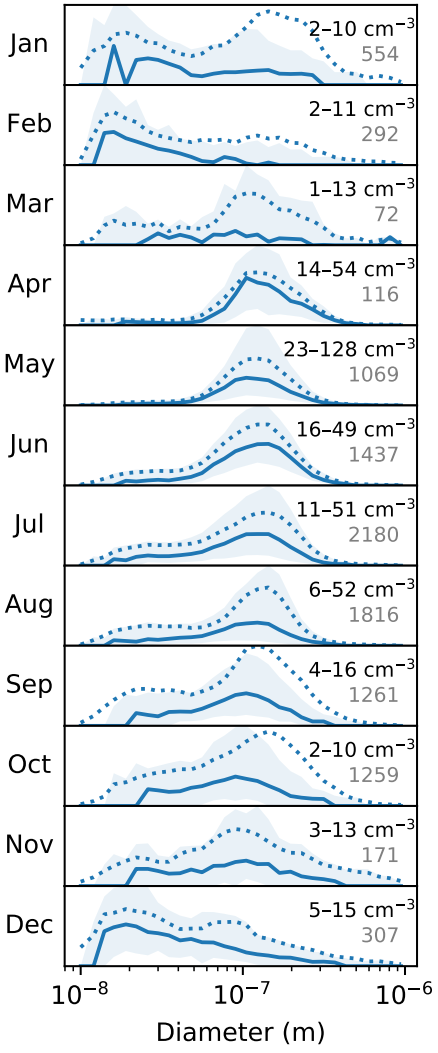

Figure S9. Monthly average cloud residual number size distributions at updraft velocities below 1 ms^{-1}. Solid and dotted lines show median and mean values, respectively, and shaded areas indicate the 25$^{\text{th}}$ to 75$^{\text{th}}$ percentile ranges. The numbers in the upper right corner of each panel indicates the 25$^{\text{th}}$ to 75$^{\text{th}}$ percentile ranges of the integrated number concentrations. The grey numbers below indicate the number of data points we have per month. The corresponding figure for all updraft velocities is shown in the main manuscript.

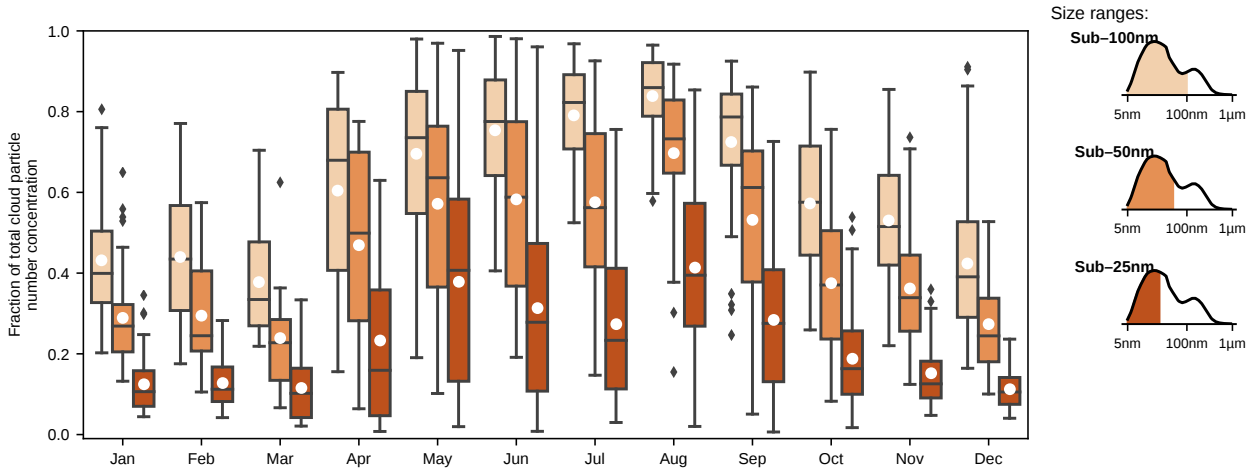

Figure S10. Contribution of small particles to the total ambient particle population. Box plot of daily average contributions (fraction of the total particle number concentration) of Aitken mode particles to the total aerosol population (both during cloud events and clear sky). The whiskers extend no more than 1.5 times the interquartile range past the edges of the box, and data points outside that range are marked by black diamonds. Mean values are indicated by white dots. The different shades of orange indicate the particle size ranges sub-100 nm, sub-50 nm and sub-25 nm diameter (see legend).

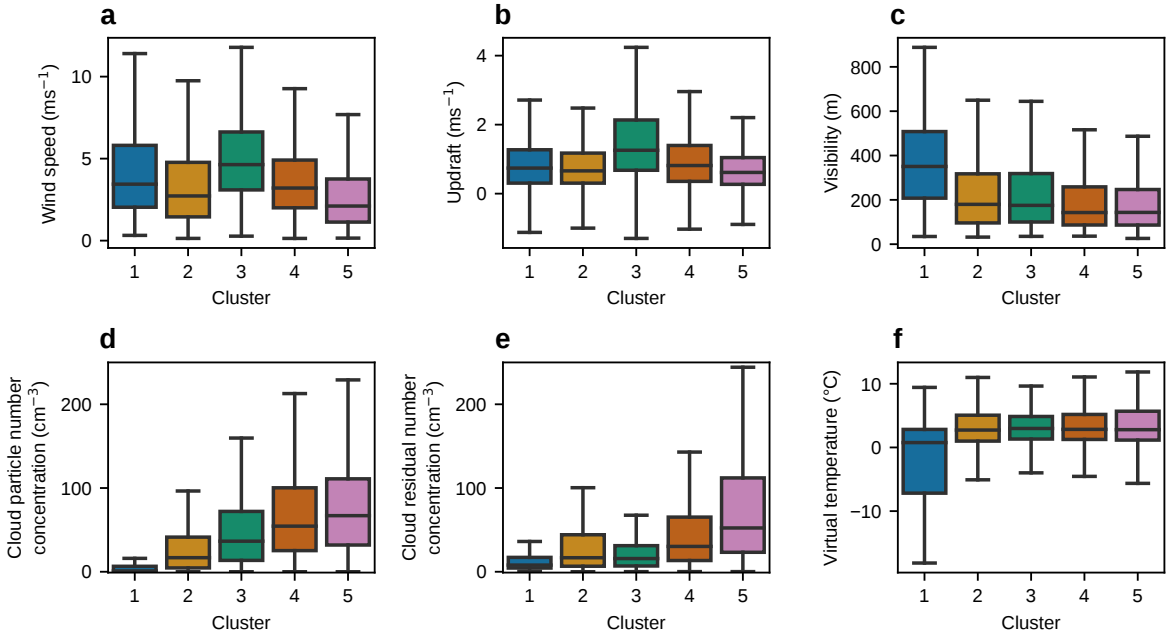

Figure S11. Additional parameters for the cluster analysis from Figure 8 in the main manuscript. The panels show the distribution per cluster of **a** wind speed, **b** updraft, **c** visibility, **d** cloud particle number concentration (without any correction factors), **e** cloud residual number concentration (corrected by CVI sampling efficiency), and **f** virtual temperature measured by the ultrasonic anemometer. Results of k-means clustering of cloud residual number size distributions using 5 clusters.

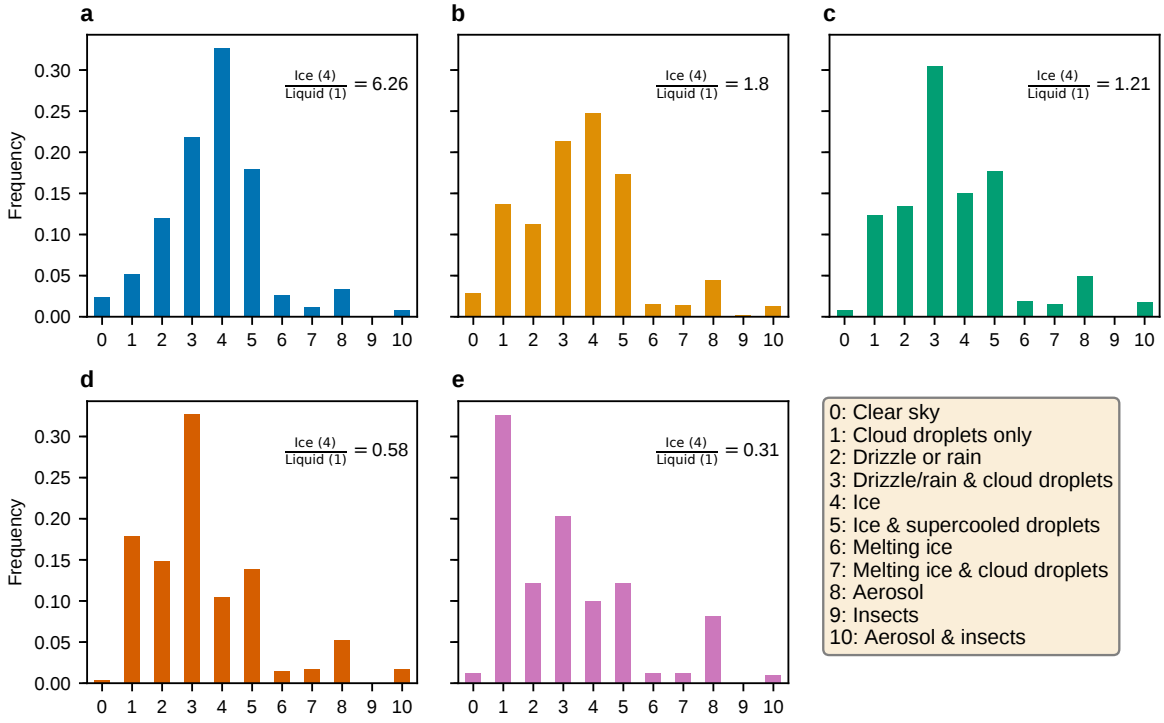

Figure S12. Cloud radar target classification for the clusters from Figure 8 in the main manuscript. Relative frequency of occurrence of different Cloudnet airmass classes (0–10, see legend). Panels **a–e** show the classifications for Clusters 1–5, respectively.

Table S1. Hours of concurrent data from different instruments. Table showing the amount of simultaneous data, rounded to the nearest hour, for different combinations of instruments. The data are divided into cloudy (i.e. GCVI on and visibility < 1 km) and clear (i.e. GCVI off and visibility > 1 km). Data combinations that are not available or not used within our analysis are marked with dashes.

	cloudy (h)	clear (h)	Relevant for
DMPS 1	1 729	–	Figs. 6, 7, S3
DMPS 2a–b	1 339	8 000	Fig. S10
DMPS 1 & FM-120	1 700	–	Figs. 2, 8, S6, S4
DMPS 1 & uSonic	1 632	–	Fig. S1
DMPS 1 & uSonic & FM-120	1 603	–	Figs. S11, S5
DMPS 1 & Cloudnet	500	–	Figs. 9, S12
DMPS 1 & DMPS 2a–b	1 136	3 684	Figs. S2, S8
DMPS 1 & DMPS 2b & uSonic	1 086	–	Fig. 5
DMPS 1 & DMPS 2a–b & FM-120	1 111	–	Fig. S7
DMPS 1 & DMPS 2a–b & FM-120 & uSonic	1 029	–	Figs. 3, 4

References

Shingler, T., Dey, S., Sorooshian, A., Brechtel, F. J., Wang, Z., Metcalf, A., Coggon, M., Mülmenstädt, J., Russell, L. M., Jonsson, H. H., and Seinfeld, J. H.: Characterisation and airborne deployment of a new counterflow virtual impactor inlet, Atmos. Meas. Tech., 5, 1259–1269, https://doi.org/10.5194/amt-5-1259-2012, 2012.